Few-body dynamics underlying postcollision effects in the ionization of H_2 by 75-keV proton impact

M. Dhital,[1] S. Bastola,[1] A. Silvus,[1] A. Hasan,[2] B. R. Lamichhane,[1] E. Ali,[1] M. F. Ciappina,[3] R. A. Lomsadze,[4] D. Cikota,[1] B. Boggs,[1] D. H. Madison,[1] and M. Schulz[1]

[1]*Department of Physics and LAMOR, Missouri University of Science & Technology, Rolla, Missouri 65409, USA*
[2]*Department of Physics, UAE University, P.O. Box 15551, Al Ain, Abu Dhabi, United Arab Emirates*
[3]*Institute of Physics of the ASCR, ELI-Beamlines, Na Slovance 2, 182 21 Prague, Czech Republic*
[4]*Tbilisi State University, Tbilisi 0179, Georgia*

(Received 10 February 2019; revised manuscript received 16 April 2019; published 24 June 2019)

We have measured fully differential cross sections (FDCS) for ionization in 75-keV $p + H_2$ collisions for ejected electron speeds close to the projectile speed. The data were analyzed in dependence on both the electron emission angle and the projectile scattering angle. Pronounced postcollisional effects between the projectile and the ejected electrons were observed. Significant differences between experiment and theory and between two conceptually very similar theoretical models were found. This shows that in the region of electron-projectile velocity-matching the FDCS is very sensitive to the details of the underlying few-body dynamics.

DOI: 10.1103/PhysRevA.99.062710

I. INTRODUCTION

One of the most important goals of ion-atom collision research is to advance our understanding of the few-body dynamics in systems consisting of a small number of charged particles [1,2]. To this end, one process which has been studied extensively, and which is also the focus of the present article, is ionization of simple target atoms or molecules by charged particle impact (for reviews see, e.g., [2,3]). The major theoretical challenge in this task is that the Schrödinger equation is not analytically solvable for more than two mutually interacting particles even when the underlying forces are precisely known. As a result, theory has to resort to numeric models and the assumptions and approximations entering in these models have to be tested by detailed experimental data.

Such numeric approaches can crudely be grouped into perturbative and nonperturbative models. The latter have the advantage that they tend to be numerically "more complete" in the sense that a large number of basis states can be included so that the influence of reaction channels other than the process of interest on the cross sections can be accounted for. As a result, ionization of simple target atoms (and other processes) by electron impact are often well described by such models (e.g., [4–6]). For ion-atom collisions nonperturbative calculations are much more challenging due to the much larger projectile mass which means that an enormous number of partial waves have to be considered to adequately describe the scattered projectile. Furthermore, the positive charge of the projectile necessitates the inclusion of projectile states in the basis sets if the effect of the capture channel is to be considered. As a result, the literature on nonperturbative calculations for ion impact (e.g., [7–10]) is not as extensive as for electron impact.

Perturbative models effectively represent two-state approximations (accounting only for the initial state and the final state observed in the experiment). In one class of perturbative models, the transition amplitude is expanded in powers of the interaction potential (Born series) [11]. One advantage of this approach is that it tends to be more transparent than nonperturbative methods to the physical mechanisms leading to the collision process. Each expansion term can be associated with a specific contribution which classically corresponds to a sequence of interactions between pairs of particles within the collision system. By comparing experimental results with theory the relative importance of the various interaction sequences in the collision dynamics can be evaluated.

The disadvantage of this expansion series approach is that in practice it has to be truncated after some order to be numerically feasible. Calculations have been carried out to second order for several processes (e.g., [12–14]), but not many attempts if any have been made to calculate third- or higher-order terms. For collision systems with relatively small perturbation parameters η (projectile charge to speed ratio) a second-order (and in some cases even a first-order) description is often sufficient; however, for large η higher-order terms can be quite important and the expansion series may not even converge at all. An alternative perturbative approach to account for higher-order contributions is offered by distorted wave methods, which treat such contributions in the final-state wave function (e.g., [15–19]). The advantage compared to the Born series is that any physical effect contained in the wave function is automatically included to all orders of perturbation theory so that the convergence problem of the Born series does not occur directly and is significantly reduced. However, it is not completely solved because it is not possible to include all the important physical effects in the wave function. Thus, these effects become part of the perturbation. Nevertheless, perturbative calculations on processes occurring in ion-atom collisions have focused on distorted wave approaches in recent years.

One higher-order mechanism that has been studied extensively is known as the postcollision interaction (PCI) (e.g., [20–26]). Here, the projectile interacts at least twice with a target electron. In the primary interaction the electron is lifted to the continuum and in the second interaction the projectile and the electron "focus" each other leading to a reduction in their relative velocity vectors. However, classically, either

the electron or the projectile needs to be redirected by a collision with the target nucleus before the second projectile-electron interaction can occur. Therefore, the two leading-order interaction sequences leading to PCI are V_{Pe}-V_{Te}-V_{Pe} and V_{Pe}-V_{PT}-V_{Pe} [27,28], where the subscripts P, T, and e stand for projectile, target nucleus, and electron. Of course, contributions of higher order containing these sequences are also possible and are accounted for in distorted wave approaches. Such focusing effects caused by PCI were found in the ejected electron energy spectra (e.g., [20,21]), in the projectile scattering angle dependence of double differential cross sections (DDCS) [22,28], as well as in recoil-ion momentum spectra [26]. These signatures maximize when the electron and projectile velocities $\mathbf{v}_e$ and $\mathbf{v}_p$ are equal to each other (matching velocity). However, especially for highly charged ion impact PCI can alter the momentum distribution of the ejected electrons significantly even far away from the matching velocity [29]. Apart from affecting the velocity vector of electrons ejected in ionization, PCI effects can also distort the line shape of autoionization following inner shell vacancy production by ionization, excitation, or capture in ion-atom collisions [30]. Finally, we note that postcollisional effects of the residual target ion on the ejected electron have been observed as well [31].

The most sensitive tests of theoretical calculations are generally offered by fully differential cross sections (FDCS) extracted from kinematically complete experiments. In the fully differential angular distribution of electrons ejected by highly charged ion impact a pronounced peak structure in the direction of the initial projectile velocity (defining $\theta_e = 0$), caused by PCI, was observed even for electron speeds much smaller than the projectile speed [23]. On the other hand, for collisions with protons or moderately charged ions only a shift of structures in the angular distribution toward $\theta_e = 0^\circ$, but no separate peak structure at $\theta_e = 0^\circ$, was found if $v_e \ll v_p$, in accordance with theoretical predictions [24,32]. In contrast, for $v_e = v_p$ calculated FDCS for 75-keV $p + H_2$ collisions were completely dominated by a sharp peak structure at $\theta_e = 0$ [33]. Surprisingly, this forward peak was nearly completely absent in experimental data [25]. One possible explanation that was considered was that the capture channel, not accounted for by perturbative models, might remove significant flux from the ionization channel, especially near $\theta_e = 0$. The presence of the capture channel could then also make the FDCS for ionization quite sensitive to the ejected electron energy (or equivalently the projectile energy loss) because its impact should sharply maximize at the matching velocity.

In this article we present a joint experimental and theoretical study of FDCS for ionization in 75-keV $p + H_2$ collisions. Earlier experiments, performed almost at the matching velocity (corresponding to an energy loss of 56.5 eV), were extended to a broader range covering electron speeds from just below to just above the projectile speed (corresponding to energy losses of 50, 53, 57, and 60 eV). In our data a clear peak structure at $\theta_e = 0$ is now observed in the FDCS. The comparison of the data with two conceptually very similar theoretical models shows that near the matching velocity the few-body dynamics becomes very sensitive to the electron speed and ejection angle.

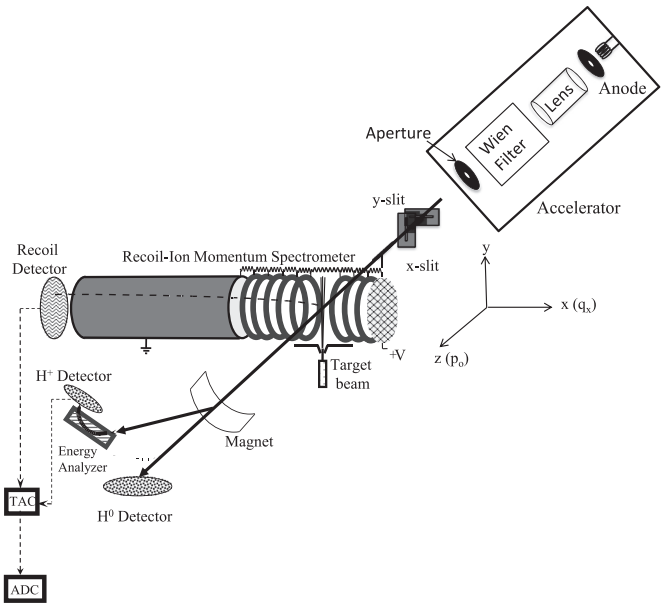

FIG. 1. Schematic sketch of the experimental setup.

II. EXPERIMENTAL SETUP

The experiment was performed at the medium energy ion accelerator at the Missouri University of Science & Technology. A schematic setup is shown in Fig. 1. A proton beam was generated with a hot cathode ion source and accelerated to an energy of 75 keV. The beam was collimated with horizontal and vertical slits, each with a width of 150 μm, placed at a distance of about 50 cm from the target region. This slit geometry, along with the projectile de Broglie wavelength of 2×10^{-3} a.u., corresponds to a transverse coherence length of about 3.5 a.u. [34]. After passing through the target region, the beam was charge-state analyzed by a switching magnet. The protons which did not undergo charge exchange were then decelerated to an energy of 5 keV and energy analyzed by an electrostatic parallel plate analyzer [35] with a resolution of 2.5 eV full width at half maximum (FWHM). The energy-analyzed projectiles were then detected by a two-dimensional position-sensitive multichannel plate detector. From the position information the projectile scattering angle θ_p was determined with a resolution of about 0.1–0.15 mrad FWHM. From the energy loss ε and θ_p the Cartesian components of the momentum transfer from the projectile to the target $\mathbf{q} = \mathbf{p}_o$–$\mathbf{p}_f$ were obtained as $q_x = p_o \tan\theta_p$ and $q_z = \varepsilon/v_p$, where the x and z axes are parallel to the analyzer slits and the initial projectile momentum, respectively (see coordinate system in Fig. 1). The y component of $\mathbf{q}$ was fixed at zero due to the very narrow width of the entrance and exit slits of the analyzer (75 μm).

In the target chamber the projectile beam was crossed with a very cold ($T \approx 1$–2 K) molecular hydrogen beam from a supersonic gas jet propagating in the y direction. The recoiling H_2^+ ions created at the intersection point between both beams were extracted in the x direction by a weak electric field ($\approx$6 V/cm) and guided onto another two-dimensional position-sensitive multichannel plate detector, which was set in coincidence with the projectile detector. The y and z

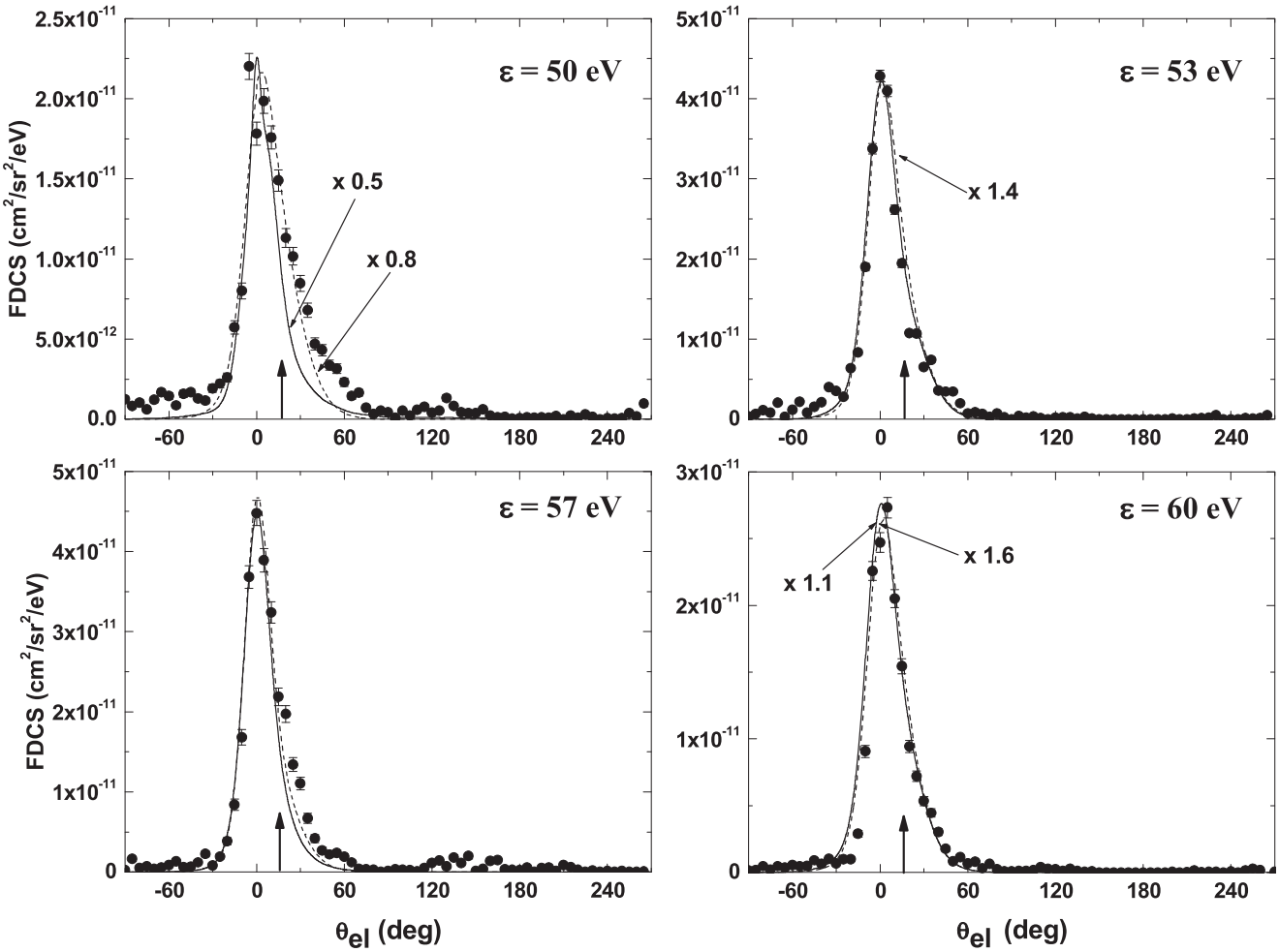

FIG. 2. Fully differential cross sections for electrons ejected into the scattering plane for a projectile scattering angle of 0.1 mrad. The projectile energy losses ε are indicated in the insets of each panel. The dashed curve represents the CDW-EIS calculation and the solid curve the 3DW calculation.

components of the recoil-ion momentum $\mathbf{p_r}$ are determined by the corresponding position components on the detector and the x component by the time of flight of the recoil ions from the collision region to the detector, which, in turn, is contained in the coincidence time.

The electron momentum was then deduced from momentum conservation as $\mathbf{p}_e = \mathbf{q}$–$\mathbf{p}_r$. The azimuthal electron emission angle is given by $\varphi_e = \tan^{-1}(p_{ey}/p_{ex})$ and the polar angle by $\theta_e = \sin^{-1}(p_{ex}/p_e)$. The magnitude of the electron momentum p_e was calculated from the energy loss (in a.u.) by $p_e = [2(\varepsilon–I)]^{1/2}$, where I is the ionization potential of H_2 (I = 15.4 eV = 0.57 a.u.). The resolution in p_e is thus determined by the energy loss resolution as $\Delta p_e = \Delta\varepsilon/p_e = 0.06$ a.u. The resolution in p_{ex} is dominated by the projectile scattering angle resolution and amounts to about 0.3 a.u. From these numbers a resolution in θ_e of about 10° FWHM was estimated for the forward direction and 13°–15° (depending on θ_p) in the direction of $\mathbf{q}$, where the so-called binary peak is expected. FDCS were analyzed for electrons of fixed energy ejected into the scattering plane spanned by $\mathbf{p}_o$ and $\mathbf{q}$ (i.e., φ_e was fixed at zero within ±5°) and plotted for fixed projectile scattering angles as a function of θ_e.

III. RESULTS AND DISCUSSION

In Fig. 2 the FDCS $= d^3\sigma/(dE_e d\Omega_e d\Omega_p)$ are plotted as a function of θ_e for $\theta_p = 0.1$ mrad and for energy losses as indicated by the insets. Here, $\varepsilon = 57$ eV corresponds to the matching speed $v_e = v_p$ (within 1%). For all four energy losses a strong peak structure at $\theta_e = 0$ is found, which becomes increasingly narrow with v_e approaching v_p (the FWHMs in order of increasing ε are 30°, 26°, 22°, and 24°). It should be noted that this width is mostly due to the binary peak, located near the direction of $\mathbf{q}$, which for small θ_p is not resolved from the forward peak. Its intensity relative to the one of the forward peak is expected to minimize at the matching speed, thus resulting in a minimized angular width. The data of our earlier study for $\varepsilon = 57$ eV [25], where this peak structure was shifted to 15°, are thus not reproduced by the present results. The reason for this discrepancy could be related to a crack in the anode of the projectile detector used in [25], which became apparent after the experiment was completed and the data were published. However, it probably started already earlier as a tiny hairline crack which went unnoticed because the signals were not yet visibly affected.

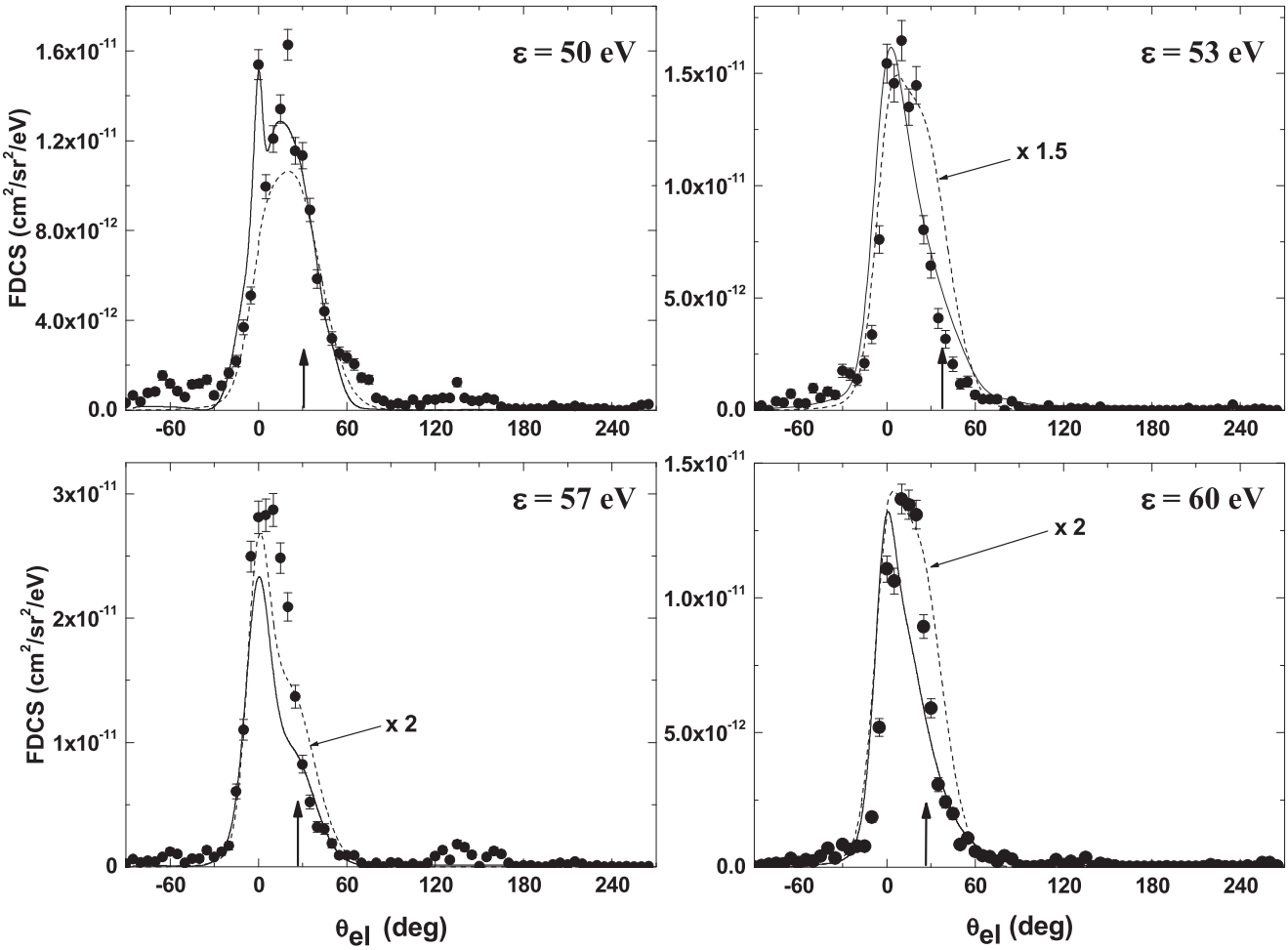

FIG. 3. Same as Fig. 2 for a projectile scattering angle of 0.2 mrad.

It nevertheless may have compromised the projectile position resolution in the x direction and thereby the corresponding component of the electron momentum.

The dashed and solid curves in Fig. 2 show our continuum distorted wave–eikonal initial state (CDW-EIS) [18] and three-body distorted wave (3DW) calculations [33], respectively. Both models represent perturbative approaches in which higher-order contributions are treated in the final-state wave function. Since the natural width of the forward peak in the calculations (varying between 2° and 10° FWHM, depending on ε) is in most cases smaller than the experimental resolution, theory had to be convoluted with the latter in order to make possible a meaningful comparison to the measured data. However, the resolution estimated in the experimental section yields theoretical peak structures which are too broad. Theory was therefore convoluted with a resolution of 5° FWHM, which for the two smaller scattering angles reproduced the half width of the negative angle wing of the peak in the experimental data very well. This suggests that our estimate of the angular resolution is too pessimistic. On the other hand, in the vicinity of the binary peak a resolution of 5° FWHM is probably too optimistic. However, the natural width of the binary peak is much larger than the experimental resolution so that here the convolution has no significant impact on the FDCS.

Both models reproduce the qualitative dependence of the measured FDCS on θ_e very well. However, in magnitude there are some differences between experiment and both theories. Furthermore, the two theories differ from each other by as much as about 40%. Since both models are conceptually very similar, this can be taken as a first indication for the FDCS being relatively sensitive to the details of the reaction dynamics in the region of the matching velocity.

In Fig. 3 the FDCS are shown for $\theta_p = 0.2$ mrad and for the same energy losses as in Fig. 2. The data still maximize near $\theta_e = 0$, but while for $\theta_p = 0.1$ mrad the FDCS are nearly symmetric around $\theta_e = 0$ (exceptfor $\varepsilon = 50$ eV), for $\theta_p = 0.2$ mrad the wing for positive θ_e is larger than the one for negative θ_e. For $\varepsilon = 50$ eV there might even be a separate peak structure at $\theta_e = 25°$, although the statistical significance of the forward peak due to a single data point $\theta_e = 0°$ is not clear. This asymmetry is a signature of an increasing contribution of the binary peak to the FDCS. The binary peak results from events in which momentum is exchanged predominantly between the projectile and the active electron (i.e., the residual target ion remains to a large extent passive) and therefore occurs near the direction of **q** (indicated in Figs. 2–5 by the vertical arrows). For ejected electron speeds much less than the projectile speed it is usually the dominant structure in the

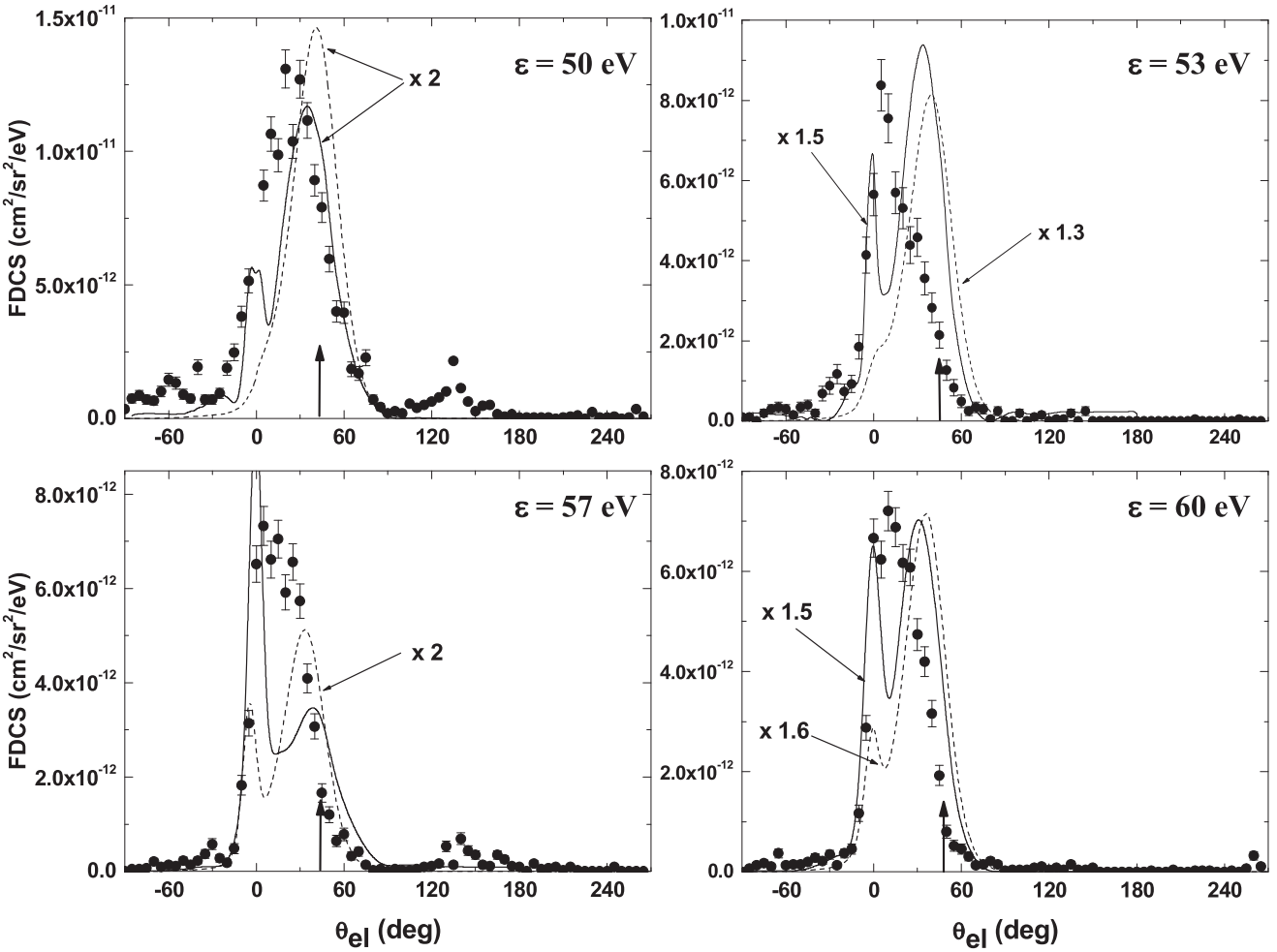

FIG. 4. Same as Fig. 2 for a projectile scattering angle of 0.325 mrad.

FDCS. For $\theta_p = 0.2$ mrad the direction of $\mathbf{q}$ is between 26° and 31° (depending on energy loss) so that the binary peak is not resolved from the forward peak (with the possible exception of $\varepsilon = 50$ eV). Rather, its contribution only leads to the aforementioned asymmetry favoring positive θ_e.

The comparison to theory reveals increasing discrepancies with the experimental data, not only in magnitude, but also in shape. Furthermore, the differences between both theories are also increased and are quite noticeable in shape as well. While the centroid of the FDCS calculated with CDW-EIS tends to be shifted to slightly larger angles than in the experimental data, for the 3DW model the centroid is shifted to smaller angles, at least for the two larger energy losses. In magnitude the differences between both calculations are now increased to as much as a factor of 2. Overall, in shape the experimental data fall somewhere between both theories. We note that the 3DW calculation yields separate forward and binary peak structures at $\varepsilon = 50$ eV, lending some credence to the measured data point at $\theta_e = 0°$.

At $\theta_p = 0.325$ mrad the contributions to the FDCS (shown in Fig. 4) from the binary peak relative to the forward peak have increased (compared to the smaller θ_p) to the extent that the data no longer maximize at $\theta_e = 0$, especially for $\varepsilon = 50$ and 60 eV. This trend is also seen in both theoretical models, where the binary peak is in most cases even clearly separated from the forward peak. At this scattering angle there are significant and qualitative discrepancies between both calculations and the measured data as well as between both models. There is some element of qualitative agreement between the theoretical results insofar as they both predict the forward to binary peak intensity ratio to maximize around $v_e/v_p = 1$ (i.e., at $\varepsilon = 57$ eV), as expected. But quantitatively, that ratio is significantly larger in the 3DW model for all ε.

The FDCS for $\theta_p = 0.55$ mrad are plotted in Fig. 5. At this scattering angle the binary peak in the experimental data is clearly separated from the forward peak, except for $\varepsilon = 57$ eV. Since at this energy loss the momentum transfer occurs at $\theta_e = 55°$ the binary peak should be separated from the forward peak. The observation that the binary peak is not at the direction of the momentum transfer points to another well-known signature of higher-order contributions: They lead to a forward shift of the binary peak relative to the direction of $\mathbf{q}$ [24]. Indeed, for the other energy losses the peak is shifted as well and the shift increases, as expected, with decreasing departure of the electron speed from the projectile speed.

A small forward shift of the binary peak is also observed in the 3DW calculations, at least for the two larger ε, but

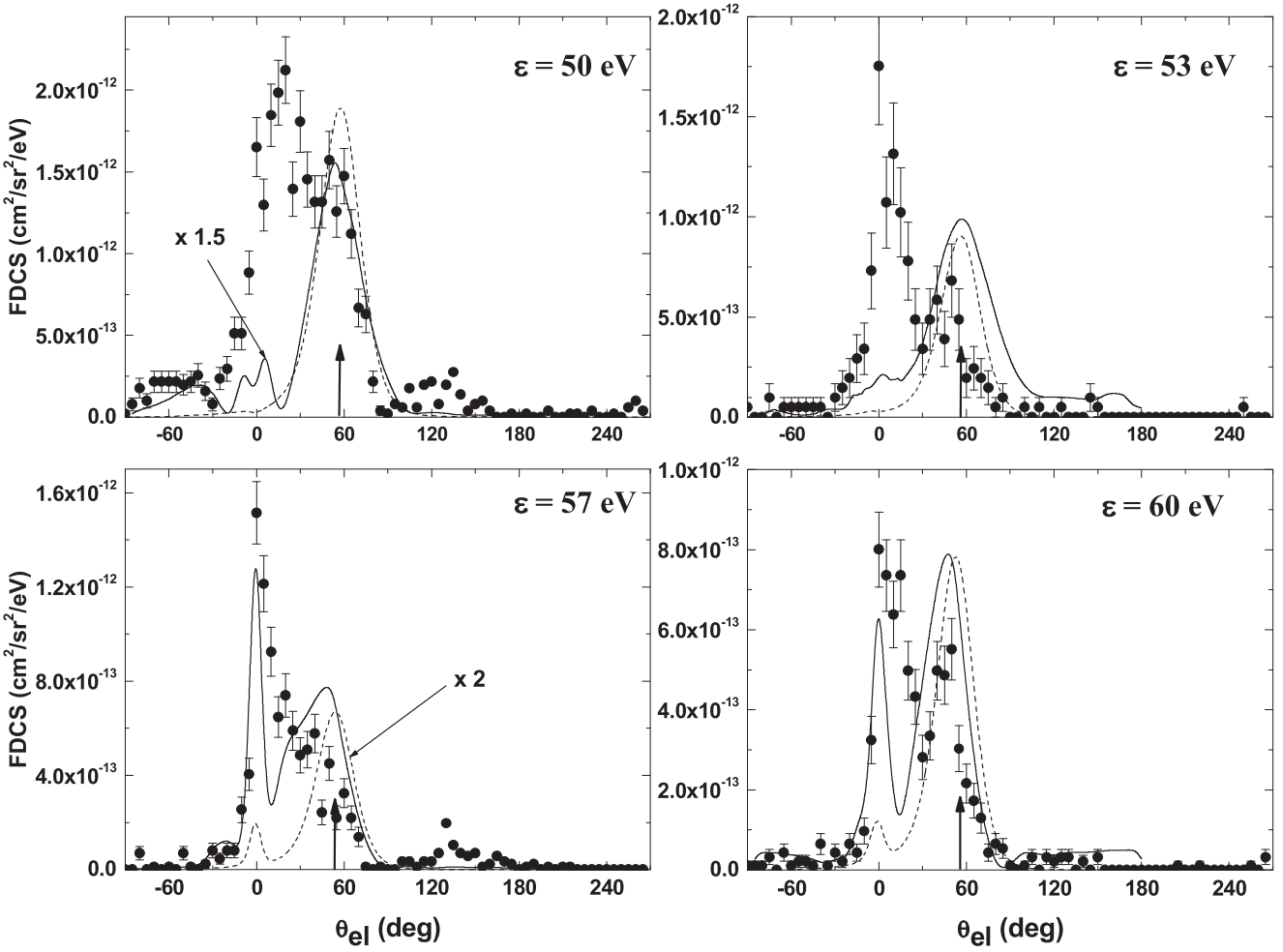

FIG. 5. Same as Fig. 2 for a projectile scattering angle of 0.55 mrad.

interestingly not in the CDW-EIS results even at $\varepsilon = 57$ eV (i.e., $v_e = v_p$). On the other hand, a small shift of about 7° is seen in the calculation for $\varepsilon = 57$ eV and $\theta_p = 0.325$ mrad. This trend in the CDW-EIS results is similar to what was measured and calculated for FDCS in 16-MeVO^{7+} + He collisions for electron speeds much smaller than the projectile speed [24]: The forward shift of the binary peak decreased with increasing transverse momentum transfer (q_{tr}) and reached a minimum at $q_{tr} \approx 1.5$ to 2 a.u., which for the present collision system corresponds to $q_p \approx 0.55$ mrad, making it even larger than in the 3DW results. In contrast, at $\varepsilon = 57$ eV the 3DW model predicts a larger forward shift for $\theta_p = 0.55$ mrad than for 0.325 mrad.

It seems plausible to associate the forward shift of the binary peak with PCI. However, it should be noted that for 16-MeVO^{7+} + He collisions studied in [24] it could be clearly traced to PCI only for $q_{tr} > 2$ a.u.. For $q_{tr} < 1.5$ a.u. this shift was explained by another higher-order mechanism involving the projectile-target nucleus (PT) interaction and an interaction of the electron, already promoted to the continuum by the projectile, with the target nucleus. On the other hand, it should also be noted that in the present work we study a very different kinematic regime. More specifically, since the electron speed is close to the projectile speed it is quite possible that even for $q_{tr} < 1.5$ a.u. (or $\theta_p < 0.5$ mrad) the forward shift of the binary peak is mostly caused by PCI.

Apart from the forward shift of the binary peak at $\theta_p = 0.55$ mrad there are also large and qualitative differences between the 3DW and CDW-EIS calculations in the binary to forward peak intensity ratio and in the overall magnitude of the FDCS; both calculations show large discrepancies compared to the measured FDCS. Considering the conceptual similarity of both models this is a very surprising observation which calls for an explanation. To this end, the conclusions obtained from a double differential study of ionization of atomic hydrogen by 75-keV p impact [28] may point in the right direction. There, it was found that in the CDW-EIS model PCI effects are predominantly caused by the V_{Pe}-V_{PT}-V_{Pe} sequence. The description of the PT interaction, occurring in this sequence, represents the perhaps most significant difference between the two models. While in the CDW-EIS approach this interaction is treated semiclassically, assuming a straight-line trajectory for the projectile and using the eikonal approximation, in the 3DW model it is accounted for fully quantum-mechanically in terms of a Coulomb factor in the final-state wave function. For a 75-keV proton it may not seem obvious that this difference is important. On the other hand, the increasing discrepancies between experiment

and theory and between both calculations with increasing θ_p show that the FDCS become very sensitive to the details of the few-body dynamics, especially at large θ_p.

Another question to be answered is why the disagreement between theory and experiment grows so large at large θ_p. Several factors may contribute to these discrepancies. First, in the case of an atomic hydrogen target it was found that in a hybrid model, referred to as second Born approximation with Coulomb waves (SBA-C), the relative importance of the two interaction sequences contributing to PCI (V_{Pe}-V_{PT}-V_{Pe} and V_{Pe}-V_{eT}-V_{Pe}) is reversed compared to CDW-EIS [28]. In the SBA-C approach the PT interaction is treated in the operator of the transition amplitude, but the higher-order contributions in the projectile-electron interaction are treated in the final-state wave function. Generally, the experimental data were in better agreement with the SBA-C than with the CDW-EIS calculations. This can be taken as an indication that the contributions from the V_{Pe}-V_{eT}-V_{Pe} sequence may be underestimated by the CDW-EIS results.

Second, in [28] it was argued that treating higher-order contributions in the projectile-electron interaction in the final-state wave function (as done in both CDW-EIS and 3DW) should be more accurate than in the Born series truncated after the second-order term. However, contributions involving the PT interaction were believed to be more adequately described in terms of the second Born approximation (as done in the SBA-C model). The reasoning for this assumption was that such higher-order contributions are expected to select events in which all three particles are relatively close together. The projectile needs to approach the electron to a close distance in order to transfer sufficient energy for ionization to occur. But the projectile also needs to approach the target nucleus rather closely for the PT interaction to play an important role. However, the final-state wave function in distorted wave approaches is known to be accurate only if at least one particle is far from the other two [36,37]. Therefore, even if the V_{Pe}-V_{PT}-V_{Pe} sequence provides the dominant contribution to PCI it may not be treated with sufficient accuracy by the CDW-EIS and 3DW models. Close encounters between the projectile and the target nucleus should be particularly important at large θ_p, which would explain the increasing discrepancies with increasing θ_p.

Furthermore, the capture channel, not accounted for in either model, may contribute to the discrepancies [32]. The flux in this channel is erroneously counted as ionization in the calculations. Discrepancies resulting from this factor should maximize at the matching velocity (i.e., for $v_e = v_p$ and $\theta_e = 0$). This seems to be indeed the case in the 3DW results for $\theta_p = 0.325$ and 0.55 mrad, but not for the two smaller scattering angles. On the other hand, the CDW-EIS approach systematically underestimates this structure. Since neither calculation accounts for the capture channel the comparison between experiment and theory does not allow for definite conclusions regarding its importance.

Finally, both theoretical models treat the projectiles as completely coherent; i.e., the transverse coherence length Δr is infinite. On the other hand, it has been demonstrated that measured cross sections can sensitively depend on Δr [38]. If Δr is significantly smaller than the effective dimension of the diffracting object (i.e., the target), any interference term

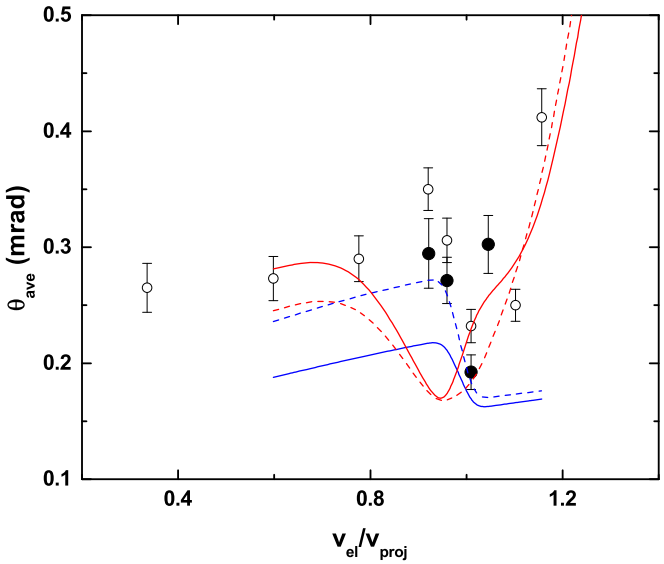

FIG. 6. Average projectile scattering angle θ_{ave} (see text) for electrons ejected at $q_e = 0$ as a function of the electron to projectile speed ratio (closed symbols). For comparison, the open symbols show θ_{ave} obtained from double differential cross sections (integrated over all electron solid angles) [28]. Dashed blue curve: CDW-EIS calculation without projectile-target nucleus (PT) interaction; solid blue curve, CDW-EIS calculation with PT interaction; red dashed curve, 3DW without PT interaction; solid red curve, 3DW calculation with PT interaction.

predicted by theory may not be observable. The effective target dimension, in turn, is basically determined by the impact parameter dependence of the reaction probability. At impact parameters larger than 3.5 a.u. (i.e., the coherence length realized in this experiment) the ionization probability is expected to be rather small. Nevertheless, it has been theoretically demonstrated that even at $\Delta r = 3.5$ a.u. the projectiles cannot be regarded as fully coherent and that the cross sections are very sensitive to Δr in this region [39].

As pointed out in the Introduction PCI represents a focusing effect between the projectile and the ejected electron in which both particles attract each other toward the initial projectile beam axis. Therefore, it should lead to a narrowing of the angular distribution of the scattered projectiles. This was indeed observed in double differential cross sections (DDCS) (in energy loss and projectile solid angle) for ionization of atomic and molecular hydrogen [28] by proton impact. On the other hand, the DDCS represent an integration of the FDCS over all ejected electron solid angles. Therefore, electrons ejected at large θ_e, i.e., those which are not affected by PCI very strongly, contribute to the width of the projectile angular distribution. An even larger narrowing effect could therefore be expected in the FDCS for θ_e fixed at 0 as a function of θ_p.

In Fig. 6 we present the average scattering angle,

$$\theta_{\rm ave} = \int (d^3\sigma/d\Omega_p d\Omega_e dE_e)\theta_p d\Omega_p \Big/ \int (d^3\sigma/d\Omega_p d\Omega_e dE_e) d\Omega_p, \quad (1)$$

for $\theta_e = 0$ as a function of the electron to projectile speed ratio v_e/v_p as closed symbols. For comparison, the open symbols represent the corresponding average angles obtained from the DDCS reported in [28]. In both data sets a pronounced minimum is observed near $v_e/v_p = 1$, confirming a pronounced focusing effect caused by PCI. Furthermore, this focusing effect indeed appears to be stronger in the FDCS than in the DDCS because the minimum is deeper and narrower. The dashed and solid blue curves in Fig. 6 show the CDW-EIS calculations with and without the PT interaction included, respectively, and the dashed and solid red curves the corresponding results of the 3DW model. Remarkably large differences between all four calculations and the experimental data are quite apparent.

First we analyze the comparison of both CDW-EIS calculations with the experimental data. Both reproduce a minimum at $v_e/v_p = 1$, but in both cases it is not as pronounced as in the measured values because for $v_e/v_p > 1$ the calculated $\theta_{\rm ave}$ rise much slower than in the experimental data. Up to the matching speed the calculation without the PT interaction is in much better agreement with experiment, while for $v_e/v_p > 1$ both curves approach each other. This suggests that within the CDW-EIS model the V_{Pe}-V_{PT}-V_{Pe} sequence becomes relatively unimportant for $v_e/v_p > 1$ and that its contribution to PCI may be overestimated for $v_e/v_p < 1$.

The 3DW results exhibit a good qualitative agreement with experiment except for the location of the minimum of the cross section for the velocity matching region. Whereas experiment finds the minimum at unity, the 3DW has a minimum at $v_e/v_p = 0.95$ and the width is much broader than in experiment. In the 3DW model the effect of including the PT interaction is significantly smaller than in the CDW-EIS model, suggesting that in the former the V_{Pe}-V_{PT}-V_{Pe} sequence plays a much less important role. Overall, the 3DW model is in satisfactory agreement with the experimental data. On the other hand, the CDW-EIS yields reasonable agreement up to, but not above the matching speed and the inclusion of the PT interaction does not lead to improved agreement. The comparison between the experimental data and both models thus reinforces the conclusion drawn from the analysis of the fully differential angular electron distributions that near the matching speed the FDCS are very sensitive to the details of the collision dynamics.

At the matching speed, PCI seems to have a much stronger effect for H_2 (even in $\theta_{\rm ave}$ obtained from the DDCS, open symbols in Fig. 6) than for helium. This was not necessarily expected because of the larger ionization potential I of helium. By considering the asymptotic case of I approaching zero one would expect PCI effects to become more important with increasing I. This scenario of an unbound electron is equivalent to the target nucleus not even being present so that neither of the two interaction sequences leading to PCI is present. The dependence of PCI effects on the target ionization potential was further investigated in a separate study for heavy targets (neon and argon) [40].

IV. CONCLUSIONS

We have measured and calculated fully differential cross sections for ionization of H_2 by 75-keV proton impact for ejected electron speeds close to the projectile speed. The data confirm a very pronounced peak structure for electrons ejected in the forward direction which was predicted by theory earlier [33]. This feature was not observed in a previous experiment for the same collision system and for similar kinematic conditions, probably due to a hairline crack in the anode of the projectile detector resulting in a compromised electron angular resolution.

The comparison between the experimental data and two conceptually very similar perturbative models shows that near the electron-projectile matching speed the fully differential cross sections are very sensitive to the few-body dynamics. Large differences are found both in the angular distributions of the ejected electrons and of the scattered projectiles. The most important difference between the 3DW and CDW-EIS models is the description of the projectile-target nucleus interaction, which is treated fully quantum-mechanically in the former and semiclassically in the latter model. It seems likely that the discrepancies between the experimental data and the CDW-EIS calculations can to a large extent be related to the description of the PT interaction. However, there are also significant discrepancies between the measured data and the 3DW calculation. This shows that either the PT interaction is not treated with sufficient accuracy in the 3DW model either or that other factors, such as the finite projectile coherence length or the capture channel not accounted for in theory, contribute to these discrepancies. One potential problem concerning the PT interaction, and which could affect both models, is that higher-order mechanisms involving the PT interaction could be quite selective on events in which all three particles approach each other to a relatively small distance. However, the three-body final-state wave function is only accurate if at least one particle is far away from the other two. To test a potential influence from this factor, calculations based on the second Born approximation and on nonperturbative approaches could be very helpful.

ACKNOWLEDGMENTS

This work was supported by the National Science Foundation under Grants No. PHY-1703109 and No. PHY-1505819. M.F.C. acknowledges support from the project "Advanced research using high intensity laser produced photons and particles" (Grant No. CZ.02.1.01/0.0/0.0/16 019/0000789) from the European Regional Development Fund (ADONIS).

[1] M. Schulz, R. Moshammer, D. Fischer, H. Kollmus, D. H. Madison, S. Jones, and J. Ullrich, Nature **422**, 48 (2003).

[2] M. Schulz and D. H. Madison, Int. J. Mod. Phys. A **21**, 3649 (2006).

[3] H. Ehrhardt, K. Jung, G. Knoth, and P. Schlemmer, Z. Phys. D **1**, 3 (1986).

[4] T. N. Resigno, M. Baertschy, W. A. Isaacs, and C. W. McCurdy, Science **286**, 2474 (1999).

[5] X. Ren, I. Bray, D. V. Fursa, J. Colgan, M. S. Pindzola, T. Pflüger, A. Senftleben, S. Xu, A. Dorn, and J. Ullrich, Phys. Rev. A **83**, 052711 (2011).

[6] J. Colgan, M. Foster, M. S. Pindzola, I. Bray, A. T. Stelbovis, and D. V. Fursa, J. Phys. B **42**, 145002 (2009).

[7] M. McGovern, D. Assafrao, J. R. Mohallem, C. T. Whelan, and H. R. J. Walters, Phys. Rev. A **81**, 042704 (2010).

[8] M. S. Pindzola, J. Colgan, F. Robicheaux, T. G. Lee, M. F. Ciappina, M. Foster, J.A. Ludlow, and S. A. Abdel-Naby, Adv. At., Mol. Opt. Phys. **65**, 291 (2016).

[9] M. Baxter, T. Kirchner, and E. Engel, Phys. Rev. A **96**, 032708 (2017).

[10] I. B. Abdurakhmanov, J. J. Bailey, A. S. Kadyrov, and I. Bray, Phys. Rev. A **97**, 032707 (2018).

[11] J. R. Taylor, *Scattering Theory: The Quantum Theory of Nonrelativistic Collisions* (Wiley, New York, 1972).

[12] O. Chuluunbaatar, S. A. Zaytsev, K. A. Kouzakov, A. Galstyan, V. L. Shablov, and Yu. V. Popov, Phys. Rev. A **96**, 042716 (2017).

[13] A. L. Godunov, C. T. Whelan, and H. R. J. Walters, Phys. Rev. A **78**, 012714 (2008).

[14] D. Belkić, Phys. Rev. A **43**, 4751 (1991).

[15] J. Fiol and V. D. Rodríguez, and R. O. Barracina, J. Phys. B **34**, 933 (2001).

[16] D. H. Madison, D. Fischer, M. Foster, M. Schulz, R. Moshammer, S. Jones, and J. Ullrich, Phys. Rev. Lett. **91**, 253201 (2003).

[17] R. T. Pedlow, S. F. C. O'Rourke, and D. S. F. Crothers, Phys. Rev. A **72**, 062719 (2005).

[18] M. F. Ciappina and R. D. Rivarola, J. Phys. B **41**, 015203 (2008).

[19] A. B. Voitkiv, Phys. Rev. A **95**, 032708 (2017).

[20] G. B. Crooks and M. E. Rudd, Phys. Rev. Lett. **25**, 1599 (1970).

[21] L. Sarkadi, J. Palinkas, A. Köver, D. Berenyi, and T. Vajnai, Phys. Rev. Lett. **62**, 527 (1989).

[22] T. Vajnai, A. D. Gaus, J. A. Brand, W. Htwe, D. H. Madison, R. E. Olson, J. L. Peacher, and M. Schulz, Phys. Rev. Lett. **74**, 3588 (1995).

[23] M. Schulz, R. Moshammer, A. N. Perumal, and J. Ullrich, J. Phys. B **35**, L161 (2002).

[24] M. Schulz, B. Najjari, A. B. Voitkiv, K. Schneider, X. Wang, A. C. Laforge, R. Hubele, J. Goullon, N. Ferreira, A. Kelkar, M. Grieser, R. Moshammer, J. Ullrich, and D. Fischer, Phys. Rev. A **88**, 022704 (2013).

[25] A. Hasan, T. Arthanayaka, B. R. Lamichhane, S. Sharma, S. Gurung, J. Remolina, S. Akula, D. H. Madison, M. F. Ciappina, R. D. Rivarola, and M. Schulz, J. Phys. B **49**, 04LT01 (2016).

[26] Th. Weber, Diploma thesis, University of Frankfurt, 1998 (unpublished).

[27] L. Sarkadi, L. Gulyas, and L. Lugosi, Phys. Rev A **65**, 052715 (2002).

[28] M. Schulz, A. C. Laforge, K. N. Egodapitiya, J. S. Alexander, A. Hasan, M. F. Ciappina, A. C. Roy, R. Dey, A. Samolov, and A. L. Godunov, Phys. Rev. A **81**, 052705 (2010).

[29] R. E. Olson, C. J. Wood, H. Schmidt-Böcking, R. Moshammer, and J. Ullrich, Phys. Rev. A **58**, 270 (1998).

[30] S. Ricz, I. Kádár, and J. Végh, J Phys., Colloq. **50**, C1-199 (1989).

[31] W. Schmitt, R. Moshammer, F. S. C. O'Rourke, H. Kollmus, L. Sarkadi, R. Mann, S. Hagmann, R. E. Olson, and J. Ullrich, Phys. Rev. Lett. **81**, 4337 (1998).

[32] A. Hasan, S. Sharma, T. P. Arthanayaka, B. R. Lamichhane, J. Remolina, S. Akula, D. H. Madison, and M. Schulz, J. Phys. B **47**, 215201 (2014).

[33] U. Chowdhury, M. Schulz, and D. H. Madison, Phys. Rev. A **83**, 032712 (2011).

[34] M. Schulz, in *Advances in Atomic, Molecular, and Optical Physics*, Vol. 66, edited by S. Yelin, E. Arimondo, and C. Lin (Elsevier, Amsterdam, 2017), p. 508.

[35] A. D. Gaus, W. Htwe, J. A. Brand, T. J. Gay, and M. Schulz, Rev. Sci. Instrum. **65**, 3739 (1994).

[36] Y. E. Kim and A. L. Zubarev, Phys. Rev. A **56**, 521 (1997).

[37] S. Jones and D. H. Madison, Phys. Rev. A **62**042701 (2000).

[38] K. N. Egodapitiya, S. Sharma, A. Hasan, A. C. Laforge, D. H. Madison, R. Moshammer, and M. Schulz, Phys. Rev. Lett. **106**, 153202 (2011).

[39] L. Nagy, F. Jarai-Szabo, S. Borbely, T. Arthanayaka, B. R. Lamichhane, A. Hasan, and M. Schulz, in *Interdisciplinary Research on Particle Collisions and Quantitative Spectroscopy*, edited by Dz. Belkic (World Scientific Publishing, Singapore, unpublished).

[40] A. Silvus, M. Dhital, S. Bastola, J. Buxton, Z. Klok, E. Ali, M. F. Ciappina, B. Boggs, D. Cikota, D. H. Madison, and M. Schulz, J. Phys. B **52**, 125202 (2019).